JOC The Journal of Organic Chemistry

Article

pubs.acs.org/joc

S-Nitrosation of Aminothiones

Joyeth B. Dorado,[†] Bogdan Z. Dlugogorski,*[,‡] Eric M. Kennedy,[†] John C. Mackie,[†] Jeff Gore,[§] and Mohammednoor Altarawneh[‡]

[†]Process Safety and Environment Protection Research Group, School of Engineering, The University of Newcastle, Callaghan, NSW 2308, Australia

[‡]School of Engineering and Information Technology, Murdoch University, 90 South Street, Murdoch 6150, WA, Australia

[§]Dyno Nobel Asia Pacific Pty Ltd., Mt Thorley Technical Centre 5, Woodlands Road, Mt. Thorley 2330, NSW, Australia

Supporting Information

ABSTRACT: Nitrosation reactions span a diverse range of applications, from biochemistry to industrially important processes. This study examines nitrosation of aminothiones in acidic solutions and re-evaluates currently accepted diffusion limits and the true nature of the nitrosating agent for nitrous acid initiated reactions. Experimental measurements from stopped-flow UV/vis spectrophotometry afforded derivation of equilibrium constants and reaction enthalpies. Apparent K_{eq} corresponds to 559−382 M^{-2} for thioacetamide (TA, 15−25 °C) and 12600−5590 M^{-2} for thiourea (TU, 15−35 °C), whereas the reaction enthalpies amount to −27.10 ± 0.05 kJ for TA and −29.30 ± 0.05 kJ for TU. Theoretical calculations via a thermochemical cycle agree well with reaction free energies from experiments, with errors of −2−4 kJ using solvation method SMD in conjunction with hybrid meta exchange−correlation functional M05-2X and high-accuracy multistep method CBS-QB3 for gas-phase calculations. The kinetic rates increase with acidity at activation energies of 54.9 (TA) and 66.1 kJ·mol^{-1} (TU) for the same temperature range, confirming activation-controlled reactions. At pH 1 and below, the main decomposition pathway for the *S*-nitroso species leads to formation of nitric oxide.

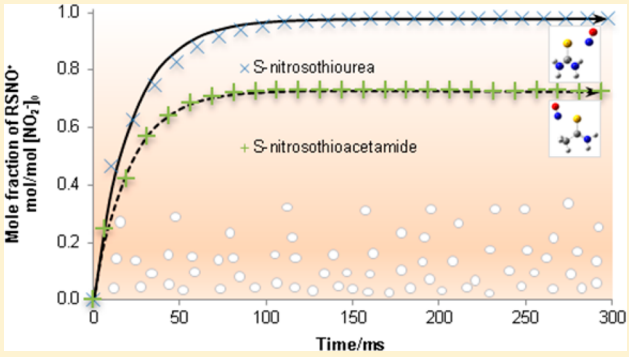

INTRODUCTION

The discovery of nitric oxide (NO) as a signaling molecule in many biological functions sparked interest in nitrosation reactions in the 1990s.[1] In recent years, continued interest in nitrosation reactions expanded to development of NO-releasing biomedical materials[2] and regulation of endogenous *S*-nitroso species[3] as well as to theoretical calculations covering these reactions and subsequent decomposition pathways.[4] Relevant applications of nitrosation reactions extend to azo pigments used in color photography and in cloth dyes[5] and also to chemical gassing of emulsion explosives in mining and construction industries. During chemical gassing of emulsion explosives, a substrate and a nitrosating agent ideally react to generate nitrogen (N_2) gas bubbles in situ, providing sensitization of the emulsion to detonation.[6,7] However, decomposition of nitrosated compounds leads to NO_x or N_2 depending on the structure of substrate. Thus, it is important to determine reaction kinetics and mechanistic pathways of nitrosation of substrates that form N_2 and NO_x for process optimization. The motivation in studying nitrosation reactions in aminothiones thiourea (TU) and thioacetamide (TA) stems from two reasons. First, nitroso-group transfer to sulfur nucleophiles was found to be more effective compared to the corresponding nitrogen or carbon nucleophiles of the same basicity,[8] and reaction at sulfur is also faster than *O*-nitrosation due to its greater nucleophilicity.[9] Second, *S*-nitrosothiol decomposition via transnitrosation to an amine group presents a potential pathway producing N_2.[10] These combined attributes of aminothiones potentially allow fast formation of N_2 where NO is not produced.

In acidic aqueous solutions, nitrous acid may form nitrosonium ion (NO^+), nitrous acidium (H_2ONO^+), and dinitrogen trioxide (N_2O_3), and the effective nitrosating agents depend highly on pH.[11−13] The ion structure of H_2ONO^+ characterizes an electrostatic complex between a free nitrosonium ion and a water molecule,[14] and it dehydrates under very acidic conditions.[15] At pH 1 and below, nitrosation proceeds via nitrosonium ion or nitrous acidium.[16]

$$H^+ + NO_2^- \rightleftharpoons HNO_2 \quad (1)$$

$$H^+ + HNO_2 \rightleftharpoons H_2ONO^+ \quad (2)$$

$$H_2ONO^+ \rightleftharpoons NO^+ + H_2O \quad (3)$$

At a much higher pH, dinitrogen trioxide (N_2O_3) from eq 4 predominates as a nitrosating agent. N_2O_3 arises as a byproduct

Received: February 10, 2015
Published: June 11, 2015

DOI: 10.1021/acs.joc.5b00313
J. Org. Chem. 2015, 80, 6951−6958

of disproportionation reaction of nitrous acid, leading to the formation of nitric oxide and nitrate through eqs 5 and 6.[17,18]

$$HNO_2 + NO_2^- + H^+ \rightleftharpoons N_2O_3 + H_2O \quad (4)$$

$$N_2O_3 \rightleftharpoons NO + NO_2 \quad (5)$$

$$NO_2 + NO_2 + H_2O \rightleftharpoons H^+ + HNO_2 + NO_3^- \quad (6)$$

For TU and substituted alkylthioureas in highly acidic solutions, eq 7 generically expresses the reversible nitrosation reaction of aminothione substrate RS forming an *S*-nitroso compound $RSNO^+$. For these species, RS is of the type $R'CSNH_2$ (e.g., R′ = NH_2, CH_3). Collings and co-workers noted that the rate law is typical of a reaction involving a nitrosonium ion with charged or neutral nucleophiles.[19] Rate constants for some alkylthioureas approach the ∼6900 $M^{-2}\cdot s^{-1}$ value for TU, implying a diffusion-controlled limit consistent with the suggestion by Ridd that reactions are dependent on the rate of encounter of an electrophile with a neutral or an anionic nucleophile.[20] Nitrosation also occurs via N_2O_3, and the rate law is second order in nitrous acid for such a case. This is well reported for nitrosation of thiols[21] and primary amines[6] but has not been studied in detail with TU and TA as substrates.

$$H^+ + HNO_2 + RS \rightleftharpoons RSNO^+ + H_2O \quad (7)$$

This study focuses on the initial *S*-nitrosation in TU and TA in acidic solutions, which are precursors to subsequent gas formation pathways. Theoretical calculations verify experimental results while gas phase analyses of products assist in elucidating the nitrosation pathways in these compounds.

RESULTS AND DISCUSSION

Four species exist in acidic conditions for nitrite-initiated nitrosation reactions: HNO_2, H_2ONO^+, NO^+, and N_2O_3. The Supporting Information discusses pH-dependent composition, with only the first three relevant at pH of 1 and lower. However, HNO_2 nitrosation in the H^+-catalyzed pathway arises only by either NO^+ or H_2ONO^+. The splitting of HNO_2 to OH^- and NO^+ requires a fairly large bond dissociation energy (918 kJ), and only proton-catalyzed heterolysis to NO^+ occurs at ambient temperatures.[14] The H_2ONO^+ pathway possibly dominates, as dehydration of nitrous acidium ion occurs only at highly acidic conditions (e.g., 45% $HClO_4$).[15] Nonetheless, both pathways involve indistinguishable rate laws, and eqs 8 and 9 represent the overall reactions.

At pH of around 2.08, Al-Mallah et al.[22] postulated, but then discounted, the direct *N*-nitrosation of TU that results in the formation of an unstable nitrosamine decomposing to nitrogen. Based on their measured rate constant of 0.2 $mM^{-1}\cdot s^{-1}$ at 25 °C and the observation that the nitrosation has no first-order dependence on acidity, Al-Mallah et al.[22] concluded that an unreasonably high pK_a for deprotonation of TU would be required at the amine site. If reaction $H^+ + HNO_2 + CS(NH_2)NH^- \rightarrow CS(NH_2)NHNO + H_2O$ proceeds at an encounter rate of 15000 $M^{-2}\cdot s^{-1}$ that is typical for anionic nucleophiles at the same temperature, section A13 of the Supporting Information demonstrates the pK_a of 4.88 for deprotonation of TU. This means that at pH of around 2.08, very little $CS(NH_2)NH^-$ exists to support a mechanism that comprises direct *N*-nitrosation of deprotonated TU. In reality, the pK_a might be even higher as seen from its tentative prediction outlined in section A3 of the Supporting Information. At pH of 3.9, da Silva et al.[6] found very good agreement between a mechanism based on *N*-nitrosation and their experimental data of decreasing nitrite ion concentration with time, but without providing spectroscopic evidence for the direct formation of the *N*-nitroso moiety. Thus, we conclude this paragraph by observing that direct *N*-nitrosation of TU is unlikely to occur at pH below 1, as investigated in this article.

$$H^+ + HNO_2 + SCNH_2CH_3 \rightleftharpoons ONSCNH_2CH_3^+ + H_2O \quad (8)$$

$$H^+ + HNO_2 + SC(NH_2)_2 \rightleftharpoons ONSC(NH_2)_2^+ + H_2O \quad (9)$$

$$HNO_2 + SC(NH_2)_2 \rightleftharpoons H^+ + SCN^- + N_2 + 2H_2O \quad (10)$$

In acidic solutions, TU and TA can be protonated at the sulfur atom. Moreover, protonation may also occur at the nitrogen atom in TU, but theoretical calculations point to sulfur site preference.[23] Taking into account this protonation equilibrium, the rate law assumes a form that simplifies back to the generic rate law for eq 7 at $K_a \gg [H^+]$ as discussed further in section A3 of the Supporting Information. The ChemAxon Marvin[24] pK_a prediction for the protonated sulfur sites is −3.0 for both TA and TU. Several studies in the past determined these pK_a's both experimentally and theoretically. For TA, Sandström[25] and Edward et al.[26] quoted values of −1.76 and around −2.5, respectively. In the case of TU, conflicting pK_a values in the literature range from −1.58 to 2.03, and Schiessl et al.[23] presented evidence that −1.3 is correct for aqueous solutions. Thus, at the pH of experiments both substrates are not protonated, and the generic rate law for eq 7 remains unaffected.

Molar Absorptivity and Equilibrium Constant. Equation 7 expresses a generic reversible nitrosation reaction of a substrate RS forming an *S*-nitroso compound $RSNO^+$. Neglecting parallel HNO_2 reactions and where $[HNO_2]_0$ depicts the initial nitrite concentration, the concentration of HNO_2 equates to $[HNO_2] = [HNO_2]_0 - [RSNO^+]$. Note that $RSNO^+$ reacts further but at a much longer time scale than that considered in this study. Equation 11 expresses a linear equation for calculation of apparent equilibrium constant K_{eq} as in the approach by Collings et al.[19] This approach applies equilibrium conditions for a reaction wherein the acid (i.e., $[H^+]$) and substrate are present in excess; i.e., $[RS] \gg [HNO_2]$ and $[H^+] \gg [HNO_2]$. From the Beer−Lambert law defining absorbance *A* in terms of extinction coefficient ε and path length *L*, plots of $1/A$ with $1/[RS]$, in section A10 of Supporting Information, yield ε and K_{eq}. Table 1 lists derived values for *S*-nitrosothioacetamide and *S*-nitrosothiourea formation at 15−25 °C and 15−45 °C, respectively.

$$\frac{1}{A} = \frac{1}{\varepsilon L[HNO_2]_0}\left[1 + \frac{1}{K_{eq}[H^+][RS]}\right] \quad (11)$$

For TU, the molar absorption coefficients up to 35 °C fall within literature values of 96 and 113 $M^{-1}\cdot cm^{-1}$.[22,27] The decreasing trend of these coefficients at higher temperatures results from the increased rate of *S*-nitrosothiourea decomposition, which interferes with the initial *S*-nitrosation. In the case of TA, the absorptivity remains stable at ∼190 $M^{-1}\cdot cm^{-1}$ with variation in temperature, ionic strength, and acidity. Although this is twice the only published value of 98 $M^{-1}\cdot cm^{-1}$, values up to 194 $M^{-1}\cdot cm^{-1}$ have been reported for *S*-nitroso adducts of alkylthioureas at the same wavelength.[22,28]

DOI: 10.1021/acs.joc.5b00313
J. Org. Chem. 2015, 80, 6951−6958

Table 1. Molar Absorption Coefficients ε at 420 nm and the Corresponding Apparent Experimental K_{eq} at 0.002 mM $NaNO_2$, 1 M $NaClO_4$, and pH 1

	thioacetamide		thiourea	
T (°C)	ε ($M^{-1}\cdot cm^{-1}$)	K_{eq} (M^{-2})	ε ($M^{-1}\cdot cm^{-1}$)	K_{eq} (M^{-2})
15	190.0	559	109	12600
20	190.0	467	109	9360
25	191.0	382	108.3	8270
30			108.2	6740
35			107.4	5590
40			106.3	4900
45			105.1	4220
ΔH^θ (kJ)	-27.1 ± 0.1^a		-29.3 ± 0.4^b	
ΔS^θ ($kJ\cdot K^{-1}$)	-0.041^a		-0.022^b	

[a]Obtained for 15−25 °C. [b]Obtained for 15−35 °C.

In both substrates, a drop in K_{eq} with increasing temperature indicates exothermicity of forward reactions. Equation 12 develops from the definition of the equilibrium constant in terms of the Gibbs free energy change ($K_t = e^{-\Delta G\theta/RT}$) and $\Delta G^\theta = \Delta H^\theta + T\Delta S^\theta$.

$$\ln K_t = -\frac{\Delta H^\theta}{R}\left(\frac{1}{T}\right) + \frac{\Delta S^\theta}{R} \tag{12}$$

Hence, the linear plot of ln K_t with $1/T$ enables calculation of standard enthalpy ΔH^θ and entropy ΔS^θ change for the reaction. These linear plots involve (true) thermodynamic equilibrium constants (K_t). However, apparent equilibrium constants (K_{eq}) serve as reasonable approximates. The enthalpy changes of reaction for both species are very close, coherent with structure similarity. For TU, interference from the decomposition pathway limits the linear plots to 35 °C, resulting in −29.3 kJ for an enthalpy change of reaction consistent with published value of −30 kJ.[19] Thermodynamically, *S*-nitrosation of TA appears less favorable with −27.1 kJ reaction enthalpy; this constitutes the first value reported for this species. Consistently, the relative entropies depict a more positive value for TU.

In solutions of high ionic concentrations, the effective concentration or activity of ionic species varies significantly from actual concentrations due to electrostatic interactions of ions and requires corrections in terms of activity coefficients. Approximate activity coefficients often employ semiempirical equations such as one proposed by Robinson and by Guggenheim and Bates[29] instead of the more involved specific interaction theory requiring empirical interaction coefficients for individual ions in the solution or the more elaborate Pitzer equation. The main difficulty in these approaches lies in accounting for the interaction of $RSNO^+$ species and the judicious use of empirical parameters in both SIT (i.e., ε_i) and Pitzer (i.e., β^0) equations. Hence, our analysis anchors on an alternate graphical approach using a simpler extended Debye−Hückel equation.[30] Table 2 illustrates an increase in the apparent equilibrium constants with ionic strength, a similar trend observed in nitrosyl thiocyanate formation.[31] This results in true thermodynamic equilibrium constants of 86 and 2270 M^{-2} for reactions 8 (for *S*-nitrosothioacetamide) and 9 (for *S*-nitrosothiourea), respectively.

Kinetic Rates of *S*-Nitrosation. Table 3 lists rate constants for *S*-nitrosation based on the reaction mechanism in Table 4, accounting for nitrous acid equilibria (eqs 1 and 4), parallel reactions (eqs 5, 6, and 10), and decomposition of *S*-nitroso species (eq 11 and eqs 13−15, Table 4). Figures 1 and 2 show typical kinetic fits of Dynafit models with experimental data. The *N*-nitrosation (eq 10) as well as subsequent decomposition pathways do not contribute to kinetics involved at pH of 1 and below. This concurs with zero detection of N_2 as well as with kinetic rates typical of decomposition of nitroso species

Table 2. Equilibrium Constants for *S*-Nitroso Compound Formation and Determination of K_t (at 25 °C) Based on

$$\ln K_{eq} = \ln K_t + \frac{1.17582\sum \nu_i z_i^2\sqrt{I}}{1+B\sqrt{I}} \text{ at } 25\ ^\circ C.$$

ionic strength, I (M)	K_{eq} (M^{-2}) (eq 8)	K_{eq} (M^{-2}) (eq 9)
0.1	142	2900
0.2	160	3200
0.3	183	3310
0.4	212	3570
1.0	380	8270
K_t	86	2270

At lower acidities of pH 1−4.6, both substrates portray similar nitrosation trends: a decrease in equilibrium concentrations of $RSNO^+$ with a drop in $[H^+]$. Under these conditions, the participation of N_2O_3 becomes increasingly significant, with rate constants for such pathways expected to approach the diffusion limit.[16] The formation of N_2O_3 (eq 4) constitutes the rate-limiting step. Nitrosation occurs sparingly above pH 3 as nitrite exists predominantly in unprotonated form. In this work, we only present the equilibrium concentrations with decreasing acidity in section A9 of the Supporting Information. Extending the Dynafit models to experimental data at pH levels higher than pH 1 did not afford meaningful outcomes due to the much slower *S*-nitrosation rates and lower equilibrium concentrations, whereby parallel effects begin to interfere with measurements. These include sulfur precipitation for TA, interference of nitrosyl thiocyanate as a decomposition byproduct of *S*-nitrosothiourea, possible *N*-nitrosation of TU, and nitrosation by N_2O_3. Moreover, fitting seven kinetic parameters that are many orders of magnitude different to seven progress curves proved inadequate in the case of TU. Hence, we only present kinetic results for pH 1 and below, electing to study the much slower decomposition process at appropriate time scales in another work.

The fitted forward and backward rate constants for eqs 8 and 9 afford calculation of the equilibrium constants, and comparison with values measured directly in Table 1 indicates good agreement, particularly for the enthalpies and entropies of reaction. Again, the more positive entropy involved in nitrosation of TU suggests that TU is a much better nucleophile in comparison to TA. This is expected as the amine site in TU is a stronger electron-donating group than the methyl site in TA, where resonance interaction is likely as in this case. Hence, the kinetic rates obtained for *S*-nitrosothiourea formation are much higher. However, the forward rate constants exceed the perceived limiting value representing the approach to a diffusion-controlled process, whereby the rate-limiting step is the formation of an encounter pair. Previous studies, for neutral substrates at 25 °C, considered this limiting value as close to 7000 $M^{-2}\cdot s^{-1}$, based on TU.[16,22] Although a previous work published a value of 11200 $M^{-2}\cdot s^{-1}$ at the same temperature for TU,[19] our current analysis results in rate constants of 24000 $M^{-2}\cdot s^{-1}$ (TU) and 15800 $M^{-2}\cdot s^{-1}$ (TA). This indicates the need for a better understanding of such discrepancy, whether it relates to the quality of kinetic data

DOI: 10.1021/acs.joc.5b00313
J. Org. Chem. 2015, 80, 6951−6958

Table 3. Kinetic Rate Constants for *S*-Nitrosation from Figures 1 and 2 and Section A7 of the Supporting Information, for eq 7)

substrate	T (°C)	k_{7f} ($M^{-2}\cdot s^{-1}$)	k_{7b} (s^{-1})	K_{eq} (M^{-2})
thiourea	15	9490	0.8	12200
	20	15300	1.8	8530
	25	24000	2.9	8270
	30	37200	5.6	6240
	35	48300	9.3	5200
	40	72000	15.1	4760
	45	91300	24.3	3760
	E_a ($kJ\cdot mol^{-1}$)	66.1[a]	ΔH^{θ} ($kJ\cdot mol^{-1}$)	−29.6[a]
			ΔS^{θ} ($kJ\cdot K^{-1}$)	−0.025[a]
thioacetamide	15	7310	12.6	582
	20	11500	23.5	487
	25	15800	40.0	391
	E_a ($kJ\cdot mol^{-1}$)	54.9	ΔH^{θ} ($kJ\cdot mol^{-1}$)	−27.7
			ΔS^{θ} ($kJ\cdot K^{-1}$)	−0.043

[a]Obtained for a temperature range of 15−30 °C.

Table 4. Reaction Mechanisms Fitted to Experimental Data

eq no.	reaction
1	$H^+ + NO_2^- \rightleftharpoons HNO_2$
4	$HNO_2 + NO_2^- + H^+ \rightleftharpoons N_2O_3 + H_2O$
5	$N_2O_3 \rightleftharpoons NO + NO_2$
6	$NO_2 + NO_2 + H_2O \rightleftharpoons H^+ + HNO_2 + NO_3^-$
thioacetamide	
8	$H^+ + HNO_2 + SCNH_2CH_3 \rightleftharpoons ONSCNH_2CH_3^+ + H_2O$
13	$ONSCNH_2CH_3^+ \rightleftharpoons N_2 + CH_3CS^+ + H_2O$
14	$2ONSCNH_2CH_3^+ \rightleftharpoons 2NO + CH_3NH_2CSSCCH_3NH_2^{2+}$
thiourea	
9	$H^+ + HNO_2 + SC(NH_2)_2 \rightleftharpoons ONSC(NH_2)_2^+ + H_2O$
10	$HNO_2 + SC(NH_2)_2 \rightleftharpoons H^+ + SCN^- + N_2 + 2H_2O$
11	$ONSC(NH_2)_2^+ \rightleftharpoons 2H^+ + SCN^- + N_2 + H_2O$
15	$2ONSC(NH_2)_2^+ \rightleftharpoons 2NO + (NH_2)_2CSSC(NH_2)_2^{2+}$

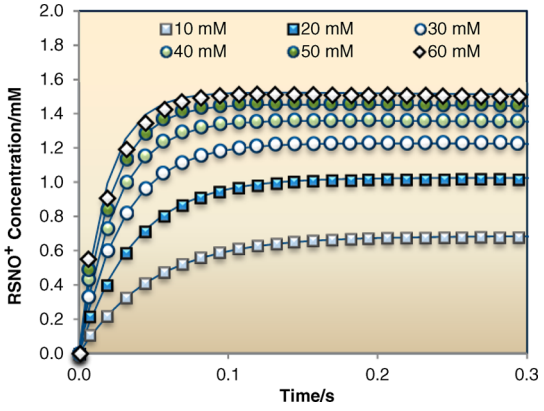

Figure 1. Concentration−time plots of *S*-nitrosothioacetamide at varying initial substrate concentrations, fitted with decomposition mechanisms at 15 °C. $[NO_2^-]_0$ = 2 mM, 0.1 M $HClO_4$ and I = 1 M, $NaClO_4$.

or the perceived limit for an encounter controlled nitrosation of a substrate with an electrophile.

Kinetic rate constants obtained in this work depend highly on the dead time, which was determined as 10.5 ms through the method of Matsumura et al.[32] for the RX2000 stopped-flow system. Particularly at higher temperatures, this dead time affords a first point of observation very close to equilibrium of $RSNO^+$ formation of less than 50 ms. For TU at 45 °C, a forward rate

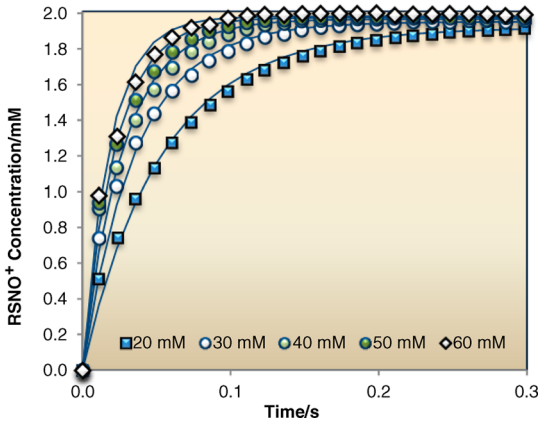

Figure 2. Concentration−time plots of *S*-nitrosothiourea at varying initial substrate concentrations, fitted with decomposition mechanisms at 15 °C. $[NO_2^-]_0$ = 2 mM, 0.1 M $HClO_4$ and I = 1 M, $NaClO_4$.

constant of 90000 $M^{-2}\cdot s^{-1}$ is obtained in comparison to 36000 and 58000 $M^{-2}\cdot s^{-1}$ based on literature values[19,22] of kinetic rates at 25 °C extrapolated using an activation energy of 64.7 $kJ\cdot mol^{-1}$. In either case, this suggests an underestimate of dead time in RX2000 if these values are taken as reference. However, the more accurate SFM3000 stopped-flow system replicates progress curves from RX2000 using the dead time included in calculations of kinetic rates, as shown in section A1 of the Supporting Information. Thus, it is an unlikely cause of the discrepancy.

To understand the basis for setting the diffusion limit for an electrophilic nitrosation, we revisit the elaborate discussion by Ridd.[33] The lack of definitive evidence for nitrous acidium ion impeded earlier attempts to resolve whether nitrous acidium (eqs 2, 16, and 17) or nitrosonium ion (eqs 18−20) embodies the active form of the nitrosating agent. An analogy is inferred for nitrosation of substrates RS by cationic nitrosating agents and in particular for nitrous acid initiated reactions in acidic media wherein the rate law is denoted by eq 21. Regardless of which nitrosation pathway occurs, eqs 17 and 20 exhibit identical rate laws. Thus, the observed rate constant in eq 17, for the nitrous acidium pathway, translates to eq 20 for the nitrosonium ion pathway, as noted in eq 21.

Nitrous acidium ($H_2NO_2^+$) pathway

$$H^+ + HNO_2 \rightleftharpoons H_2ONO^+ \quad (2)$$

DOI: 10.1021/acs.joc.5b00313
J. Org. Chem. 2015, 80, 6951−6958

$$H_2ONO^+ + RS \rightleftharpoons RSNO^+ + H_2O \quad (16)$$

$$d[RSNO^+]/dt = k_{16}[H_2ONO^+][RS] = k_{16}K_2[H^+][HNO_2][RS] = k_{7f}[H^+][HNO_2][RS] \quad (17)$$

Nitrosonium ion (NO^+) pathway

$$H^+ + HNO_2 \rightleftharpoons NO^+ + H_2O \quad (18)$$

$$NO^+ + RS \rightleftharpoons RSNO^+ \quad (19)$$

$$d[RSNO^+]/dt = k_{19}[NO^+][RS] = k_{19}K_{18}[H^+][HNO_2][RS] = k_{7f}[H^+][HNO_2][RS] \quad (20)$$

$$k_{7f} = k_{19}K_{18} = k_{16}K_2 \quad (21)$$

Ridd argued in favor of the nitrosonium ion pathway and presented calculations for singly charged anions wherein the limiting value for k_{7f} was deduced ($k_{19} \times K_{18}$) as 2500 $M^{-2}\cdot s^{-1}$ at 0 °C. The equilibrium constant of nitrosonium formation was 2.8 $\times 10^{-7}$ M^{-1} after taking into account the effect of electrostatic interaction on frequency of encounters of charged reactants (see section A11 in the Supporting Information for calculations). This was thought to be in concurrence with the 3×10^{-7} obtained of Bayliss et al.[15] using acidity function H_r to treat the equilibrium in perchloric acid.[16,33] However, the latter dimensionless equilibrium constant takes into account the presence of water in eq 18. In the same work by Bayliss, use of activities to calculate the equilibrium resulted in 8.7 and 7.6×10^{-7} at 3.5 and 15 °C for perchloric acid, respectively, and $1.7-3.0 \times 10^{-5}$ at 4.5−25 °C for sulfuric acid. Becker et al.[34] published a lower value of 1.2×10^{-8} at 25 °C in close agreement with 1.4×10^{-8} from the earlier work by Seel and Winkler.[35] Extending the same approach to 25 °C with the more consistent value by Becker, a diffusion limit for *S*-nitrosation of $k_{7f} = 1.7$ $M^{-2}\cdot s^{-1}$ is obtained for neutral substrates at acidities close to 1 M perchloric acid. Observed kinetic rate constants for such substrates exceed this value by several orders of magnitude. Although incorporating the effect of attractive electrostatic interaction for univalent ions increases this diffusion limit by a factor of ~2.6, such an increase will not be sufficient to account for the variation. Thus, it is evident that NO^+ pathway cannot account for the supposed diffusion limit of an electrophilic nitrosation process.

Recently, Anastasio et al.[12] showed spectroscopic evidence for the nitrous acidium ion, which further supports its role as an active nitrosating agent. This form constitutes more than 83% of nitrous acid for pH 1 based on dissociation constants of nitrous acid and nitrous acidium as 3.3 and 1.7, respectively.[11] If $H_2NO_2^+$ functions as the reactive species, eq 17 equivalently translates to an observed diffusion limit of 3.7×10^{11} $M^{-2}\cdot s^{-1}$ for k_{7f} (= $k_{16} \times K_2$) in eq 17 at 25 °C (Supporting Information). Although this value appears very high, the rate constant for diffusion limit results from several assumptions discussed by Ridd and translates to an upper limit.[33] One assumption presumes that the molecules adopt a uniformly reactive surface, which represents a crude approximation that could reduce the rate coefficient by one or several orders of magnitude. Certainly, the observed rate constants obtained for TU and TA do not approach the expected encounter limit for electrophilic nitrosation of neutral substrates and this indicates that the reactions are not diffusion-controlled. Thus, nitrous acidium ion appears to constitute the nitrosating species in the present experiments. This conclusion also accords with the results of the speciation calculations of Figure A-14 in the Supporting Information that yields $H_2NO_2^+$ as the predominant nitrosating species for −0.9 < pH <1.5.

As follows from the temperature dependence of the Arrhenius equation, the rate increases by a factor of 2.2−2.5 from 15 to 25 °C. The 66.1 kJ·mol^{-1} activation energy of *S*-nitrosothiourea conforms with the 65 kJ·mol^{-1} reported by Collings et al.[19] and slightly exceeds the 61 kJ·mol^{-1} obtained by da Silva et al.[6] *S*-Nitrosothioacetamide requires a lower activation energy of 54.9 kJ·mol^{-1}. Kinetic models adopt the generic rate law despite the strong likelihood that nitrous acidium is the nitrosating agent to avoid integrating errors associated with the equilibrium constant for nitrous acidium formation in calculation of kinetic rates at different temperatures. A discussion in the Supporting Information shows that the term defining the molar absorption coefficient for $RSNO^+$ species is identical for both the generic rate law and the nitrosonium ion pathway. It also derives a convenient relation defining activation energies for the latter pathway in terms of the generic rate law. The corrected activation energies are 64.6 and 75.8 kJ·mol^{-1} for *S*-nitrosothioacetamide and *S*-nitrosothiourea, respectively, and remain consistent with reaction controlled processes. The corrections are based on eq A6-9, accounting for K_a in eq A6-6 (pertaining to nitrous acidium formation in eq 2), whereby ΔG^θ is taken as −9.7 kJ mol^{-1} (from pK_a of −1.7 for H_2ONO^+ dissociation).

Theoretical Calculations. Figures 3 and 4 describe gas-phase relative free energies and geometries of conformational

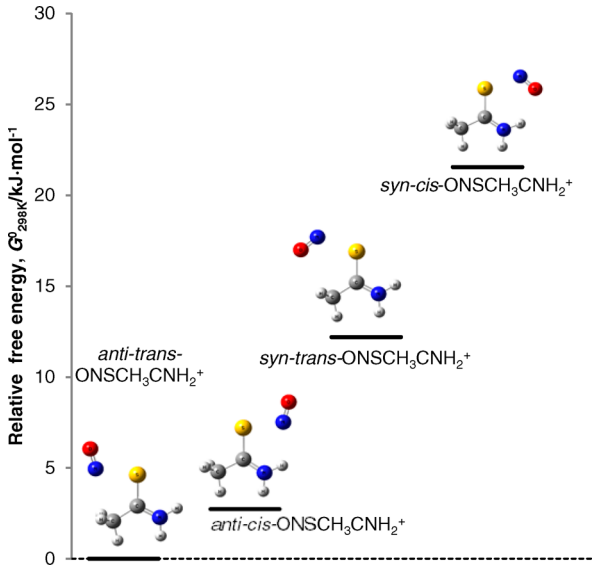

Figure 3. Gas-phase free energies of $ONSCH_3CNH_2^+$ isomers relative to *anti,trans*-$ONSCCH_3NH_2^+$, computed at the B3LYP/6-31+G(d,p) level.

isomers of $ONSCCH_3NH_2^+$ and $ONSC(NH_2)_2^+$, respectively. The energies of *cis*-nitrosothioacetamide exceed those of *trans* conformers. All stable $ONSCCH_3NH_2^+$ isomers adopt planar structures with the lowest energy for *anti-trans*-$ONSCCH_3CNH_2^+$ and *anti-trans*-$ONSCCH_3CNH_2^+$ exceeding the lowest state by 2.7 kJ·mol^{-1}. The 12 and 22 kJ·mol^{-1} higher energies for the corresponding *syn* configurations indicate negligible concentrations at equilibrium. Similarly, *syn*-$ONSC(NH_2)_2^+$ is 8.6 kJ higher than *anti* structure and this conformer

DOI: 10.1021/acs.joc.5b00313
J. Org. Chem. 2015, 80, 6951−6958

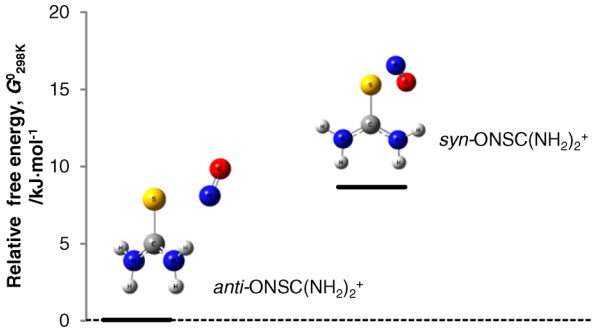

Figure 4. Relative free energies of $ONSC(NH_2)_2^+$ isomers, computed at the B3LYP/6-31+G(d,p) level.

likely exists in a small fraction during nitrosation. Geometry optimization of *syn*-$ONSCCH_3NH_2^+$ resulted in an imaginary frequency for all three methods used, whereas we located stable structures for both *anti* and *syn* configurations of $ONSC(NH_2)_2^+$. Similarly, Timerghazin et al.[36] showed that the simplest *S*-nitrosothiol HSNO favors *anti* conformation using CCSD and CCSD(T) couple cluster methods by approximately 4 kJ·mol^{-1}, while Ruano et al.[37] found, opposite to the present result, that *syn* conformers for methyl thionitrite are less energetic by 3.6−4.7 kJ·mol^{-1} in comparison to the *anti* configuration.

The change of Gibbs free energies for gas-phase nitrosation of TA and TU implies endoergic reactions. Table 5 presents

Table 5. Reaction Free Energies ΔG^{θ}_{aq} for $RSNO^+$ Formation, 25 °C

methods	ΔG^{θ}_{aq} (kJ) (eq 8)	ΔG^{θ}_{aq} (kJ) (eq 9)
experiment	−11.0	−19.1
(1) CPCM (UAHF)	−0.4	−16.5
(2) IEFPCM (Bondi)	−17.7	−22.5
(3) SMD/B3LYP	−22.1	−26.6
(4) SMD/M05-2X	−14.2	−15.5

calculated aqueous free energies based on a thermochemical cycle. The difference of −2−10 kJ and 5−7 kJ from experimental values for CPCM and IEFPCM methods complement MUEs from literature. Solvation model SMD in conjunction with B3LYP shows a systematic underestimate of 10−12 kJ. Using hybrid meta exchange-correlation functional M05-2X resulted in excellent agreement with errors dropping to −2−4 kJ. For all nitrosated substrates, the cationic structures exhibit elongated S−N bonds of around 2.1 Å for both gas- and aqueous-phase calculations that are indicative of very weak bonds. These S−N bond lengths exceed 1.7−1.9 Å commonly found in neutral *S*-nitroso species like HSNO and methyl thionitrite using theoretical calculations as well the crystallographic data for organic thionitrites.[36,37]

In addition to calculating thermochemical terms, we compare relative tendencies of TU and TA to undergo nucleophilic NO^+ *S*-addition based on their Fukui indices[38] for nucleophilic attack, f^+. According to the Fukui frontier molecular orbital theory,[39] Fukui indices relate the reactivity of a system toward a nucleophilic attack with its electronic density. Our calculated f^+ indices for S atoms in nonprotonated TU ($SC(NH_2)_2$) and TA ($SCNH_2CH_3$) amount to 0.380 and 0.334, respectively. This clearly confirms that TU is more susceptible for a nucleophilic NO-S attack than TA. The distinct difference between TU and TA stems from the fact that the amine group in TU as a stronger donating group (EDG) by resonance if compared with the methyl group in TA. On the basis of Hirshfeld's scheme,[40] we calculate slightly more negative partial charge on the S atom in TU in reference to TA, i.e., −0.301 *e* versus −0.241 *e*. These values coincide with the nature of amine group as a stronger EDG by resonance.

Decomposition Products. The early work of Werner[41] proposed that decomposition of aliphatic $RSNO^+$ moiety results in the formation of disulfide $(RSSR)^{2+}$ and nitric oxide (eqs 14 and 15, Table 4). Collings et al.[27] observed that this reaction involves a rate law whereby the first term represents a reaction between the free substrate and the *S*-nitroso adduct, while the second term corresponds to a simple bimolecular reaction of two $RSNO^+$ molecules contributing to the second-order kinetics[19] as in the case of TU. In a parallel decomposition pathway, a subsequent intramolecular transnitrosation of *S*-nitrosothiourea may occur to form N_2, a pathway proposed to dominate at lower acidities and be largely irreversible (eq 11 in Table 4). Results of NO_x chemiluminescence analysis in Figure 5 show that

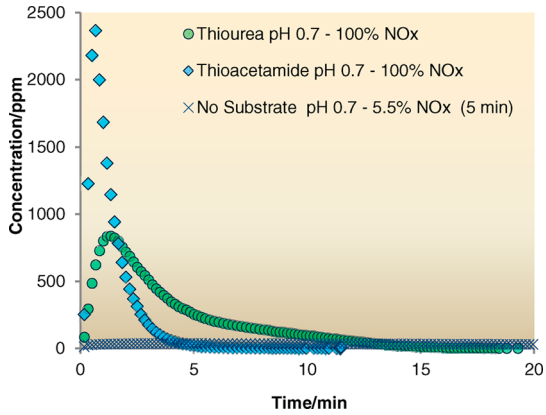

Figure 5. Comparative NO_x yields during decomposition of *S*-nitrosothioacetamide and *S*-nitrosothiourea, headspace sampling at 26 °C and pH 0.7. $[TA]_0$ or $[TU]_0$ = 10 mM and $[NO_2^-]_0$ = 1 mM, all at 1 M, $NaClO_4$.

decomposition to NO proceeds at a much faster rate for *S*-nitrosothioacetamide. Under the same conditions, nitrous acid disproportionation to NO accounts for less than 6% in 5 min where the yield is more than 80% for both substrates. Moreover, no N_2 product has been detected using micro-GC at this acidity. This precludes *N*-nitrosation at the amine sites as well an intramolecular transnitrosation as this would have resulted in subsequent formation of N_2 in either case. At pH 1 and below, formation of NO constitutes the dominant decomposition pathway of the *S*-nitrosothioacetamide and *S*-nitrosothiourea.

CONCLUSION

Thermodynamically, *S*-nitrosation of TA occurs less favorably at a reaction enthalpy of −27.7 kJ compared to −29.6 kJ for TU. The more positive entropy involved for nitrosation of TU suggests that it is a better nucleophile, in coherence with its stronger electron donating amine group as opposed to the methyl group in TA. This is further supported by the much higher Fukui index for thiourea and thus higher susceptibility for nucleophilic attack. Apparent equilibrium constants increase with ionic strength and, accounting for ionic effects, translate to thermodynamic equilibrium constants of 86 and 2269 $M^{-2}\cdot s^{-1}$ for TA and TU, respectively, at 25 °C. Equivalent reaction Gibbs

DOI: 10.1021/acs.joc.5b00313
J. Org. Chem. 2015, 80, 6951−6958

free energies concur with theoretical calculations with errors as low as ±4 kJ for the SMD/M05-2X method. In terms of kinetics, the formation of *S*-nitrosothiourea entails a much higher kinetic rate constant of 24000 $M^{-2}\cdot s^{-1}$ in contrast with the 15800 $M^{-2}\cdot s^{-1}$ constant for the generation of *S*-nitrothioacetamide at 25 °C. These values exceed the current perceived encounter limit for diffusion-controlled electrophilic nitrosation of neutral species. Revisiting the analysis of the true nature of nitrosating agent establishes that nitrosation occurs via the nitrous acidium pathway at around pH 1. Moreover, the expected encounter limit for this pathway exceeds the observed kinetic rate constants in literature by several orders, and reactions do not occur in diffusion-controlled regimes. Reaction rates increase with temperature at activation energies of 54.9 and 66.1 $kJ\cdot mol^{-1}$ for the formation of *S*-nitrosothioacetamide and *S*-nitrosothiourea, respectively, confirming that such processes occur within a reaction control regime. Finally, these *S*-nitroso species are short-lived, with the main decomposition pathways leading to scission of the S−N bond to release NO at pH 1 and below.

EXPERIMENTAL SECTION

Materials. The substrates deployed in experiments consist of TU and TA prepared fresh prior to experiments. Nitrous acid served as a nitrosating agent, made by dissolving 99.5% free-flowing sodium nitrite in solutions where perchloric acid was in excess (i.e., $[H^+] \gg [HNO_2]$). Perchloric acid was received at 70% and standardized by titration with sodium carbonate, while 98% anhydrous sodium perchlorate was stored in a desiccator prior to use. Initial substrate concentrations vary from 10 to 100 mM with the nitrite kept at 2 mM for measurements covering a temperature range of 15−45 °C at 5 °C increments. In studying effects of ionic strength, experimental conditions span 0.1−0.4 M (0.1 M increment). All solutions were prepared using distilled deionized water, with application of sodium perchlorate to maintain the solutions at the required ionic strength.

Liquid-Phase Analysis. Applied Photophysics RX2000 stopped-flow mixing accessory interfaced with a spectrophotometer allows kinetic studies for nitrosation reactions using a 1 cm path length quartz cuvette. A Peltier temperature controller regulates the temperature in the mixing cell, while a water bath thermostats the stopped-flow mixing circuit to 0.1 °C. The dead time of the stopped-flow system is determined through the method of Matsumura et al.[32] using the second-order reaction of 2,6-dichloroindophenol (DCIP) with ascorbic acid originally proposed by Nakatani and Hiromi.[42] Degassing all solutions of TA and TU with nitrogen for at least 15 min prior to experiments ensures anaerobic conditions. The signals at 420 nm form the basis for studying these reactions to avoid interference from absorption of nitrous acid and buffers at lower wavelengths as in related literature.[19,22] Furthermore, traces of copper ions in solution potentially inhibit proton addition at either the nitrogen or sulfur atom.[43] With a need to apply EDTA to remove these ions, separate experiments ascertained negligible effect of EDTA addition on *S*-nitrosation.

Gas-Phase Analysis. In situ experiments allow quantitative detection of N_2 and NO/NO_x by a headspace sampling technique. Nitrosation reactions proceed in aqueous phase within a 10 mL reactor and gaseous products exit the reactor using high purity helium (99.999%) as the mobile phase at a flow rate of 1.33 $mL\cdot s^{-1}$, allowing detection sensitivity up to 10 ppm for N_2. The initial concentrations of [TA] or [TU] were set to 10 mM and $[NO_2^-]$ to 1 mM at an acidity of 0.2 M $HClO_4$ and ionic strength of 1 M $NaClO_4$ for the 10 mL solution volumes. All reagent solutions sparged prior to mixing. Thermo 421HL NO_x chemiluminescence analyzer measures concentrations as low as 1 ppm in situ. A 1000 ppm of NO standard from Coregas Pty Ltd. calibrates this analyzer at the same set flow rate as that employed in experiments.

A microgas chromatograph quantitates N_2 and Ar−O_2 through gas separated on a Molsieve 5 Å column and H_2O from a PoraPLOT Q column, both equipped with thermal conductivity detectors, and column/injection temperatures kept at 80 °C. Measurements taken at an interval of 2.25 min monitor Ar−O_2, N_2, and H_2O at elution times of 0.91, 1.19, and 0.845 min, respectively, with a sample time of 30 s, run time of 80 s, and stabilizing time of 5 s. A system consisting of a Nafion dryer installed in the sampling line removes moisture, while N_2 purge gas flows in a countercurrent direction at 4.7 mL s^{-1}. Zero chemiluminescence detection with NO calibration gas in the purge stream rules out cross contamination between purge and sample streams within the dryer. Flow checks at the exit of the Nafion dryer confirmed no leak within the sample stream. For experiments carried out in anaerobic conditions, sparging with carrier gas removes oxygen and leak tests guarantee a well-sealed system. At least three replicates establish gas formation trends.

Data Analysis. The Dynafit program[44] fits the defined reaction mechanisms with the kinetic data obtained to determine the rate constants for *S*-nitrosation. This program uses the Levenberg−Marquardt algorithm for nonlinear least-squares regression to minimize the error between reaction progress curves and a system of first-order differential equations generated from the model reaction mechanisms. Dynafit models incorporate reaction mechanisms with known rate constants quoted from literature. Adopting the same approach used by da Silva et al.[20] and Rayson et al.[45] for protonation equilibrium, the association rate constant of nitrous acid (eq 1) assumes a value of 10^{10} $M^{-1}\cdot s^{-1}$. Variation in initial estimates of kinetic rate constants tests convergence to a global minimum.

Computational Methods. A thermochemical cycle discussed further in the Supporting Information enables calculation of the Gibbs free energy change of reaction (ΔG^{θ}_{aq}) in solution phase for cationic *S*-nitroso adducts of TU and TA from nucleophilic attack on the nitrosonium cation or nitrous acidium. This theoretical result provides a basis for comparison with the Gibbs free energy founded on experimentally obtained thermodynamic equilibrium constants K_t. In the theoretical calculations, the gas-phase free energy of formation of H^+ adopts a value of -26.3 $kJ\cdot mol^{-1}$, and the free energy of solvation of H^+ refers to the value of -1104.5 $kJ\cdot mol^{-1}$ (1 atm gas-phase standard state) from the work of Tissandier et al. using cluster-ion solvation data.[46,47] For HNO_2, the average free energy of the two isomers (*cis* and *trans*, because of partially double-bond nature of the N−O bond) applies in the calculations as in the work of Rayson et al.[48] Calculations of energy changes in a gas-phase reaction employ high-accuracy multistep methods CBS-QB3 and G3(MP2B3) with mean absolute deviations from experiments of determined previously as 4.6 and 5−5.4 $kJ\cdot mol^{-1}$, respectively.[49]

Estimated free energies of solvation display profound dependency on the deployed theoretical method as well as the utilized basis set. For instance, calculated free energies of solvation by high-level composite methods are not systematically more accurate than the corresponding values obtained by DFT functionals or even at the HF method. Thus, we elect to calculate solvation energies using different theoretical approaches. Considering ionic species in aqueous solutions, three solvation models are selected for use with gas-phase free energies to calculate free energy in the solution: conductor-like polarizable continuum model (CPCM) with united atom for Hartree−Fock (UAHF) definition for molecular cavity, integral equation formalism polarizable continuum model (IEFPCM[50,51]) in conjunction with Bondi's definition for atomic radii,[50] and solvation model[51,52] using charge density (SMD: solvation model based on density), all computed using the B3LYP functional with 6-31+G(d,p) basis set and a further hybrid meta exchange-correlation functional M05-2X for SMD. The solvation free energy required calculations performed at the same level of theory and basis set size for both solvent and gas-phase models. Conformational variations with locally stable configurations determined in the gas phase subsequently apply as the initial geometries for DFT optimization in the aqueous phase. Moreover, geometry optimization comprises both gas and aqueous phase calculations to account for any geometry relaxation upon solvation. The absence of imaginary frequencies confirmed the existence of true minima. All calculations involved the Gaussian09 program.[53] We carried out calculations of Fukui indices[38] for nucleophilic attack and electronic partial charges with the DMol^3 code.[54]

DOI: 10.1021/acs.joc.5b00313
J. Org. Chem. 2015, 80, 6951−6958

■ ASSOCIATED CONTENT

Supporting Information

Determination of dead time in stopped-flow system, typical UV−vis spectra, effect of EDTA addition, derivation of cited equations, kinetic data, calculated geometries and frequencies, ionic effects on activities, and list of experiments. The Supporting Information is available free of charge on the ACS Publications website at DOI: 10.1021/acs.joc.5b00313.

■ AUTHOR INFORMATION

Corresponding Author

*Fax: (+) 61 8 9360 6346. E-mail: b.dlugogorski@murdoch.edu.au.

Notes

The authors declare no competing financial interest.

■ ACKNOWLEDGMENTS

This study was funded by the Australian Research Council and Dyno Nobel Asia Pacific Pty Ltd., with support of computational resources from the National Computational Infrastructure (NCI) and The Pawsey Supercomputing Centre in Perth. J.B.D. thanks Edwin Romano, as well as Drs. Mark Rayson and Clovia Holdsworth, for the helpful discussions.

■ REFERENCES

(1) Singh, R. J.; Hogg, N.; Joseph, J.; Kalyanaraman, B. *J. Biol. Chem.* **1996**, *271*, 18596.
(2) Coneski, P. N.; Rao, K. S.; Schoenfisch, M. H. *Biomacromolecules* **2010**, *11*, 3208.
(3) Joslin, J. M.; Reynolds, M. M. *ACS Appl. Mater. Interfaces* **2012**, *4*, 1126.
(4) Koppenol, W. H. *Inorg. Chem.* **2012**, *51*, 5637.
(5) Hart, H. *Organic Chemistry: A Short Course*, 8th ed.; Houghton Mifflin Co.: Boston, 1991.
(6) da Silva, G.; Dlugogorski, B. Z.; Kennedy, E. M. *Chem. Eng. Sci.* **2006**, *61*, 3186.
(7) Nie, S. Doctoral Thesis, Comprehensive Summary (Other Scientific), KTH Royal Institute of Technology, 1997.
(8) Adam, C.; Garcia-Rio, L.; Leis, J. R. *Org. Biomol. Chem.* **2004**, *2*, 1181.
(9) Dix, L. R.; Williams, D. L. H. *J. Chem. Soc., Perkin Trans. 2* **1984**, 109.
(10) Adam, C.; Garcia-Rio, L.; Ribiero, L.; Leis, J. R. *J. Org. Chem.* **2005**, 6353.
(11) Riordan, E.; Minogue, N.; Healy, D.; O'Driscol, P.; Sodeau, J. R. *J. Phys. Chem. A* **2005**, *109*, 779.
(12) Anastasio, C.; Chu, L. *Environ. Sci. Technol.* **2009**, *43*, 1108.
(13) Crugeiras, J.; Ríos, A.; Maskill, H. *J. Phys. Chem. A* **2011**, *115*, 12357.
(14) Wu, H.; Glaser, R. *J. Phys. Chem. A* **2003**, *107*, 11112.
(15) Bayliss, N.; Dingle, R.; Watts, D.; Wilkie, R. *Aust. J. Chem.* **1963**, *16*, 933.
(16) Williams, D. L. H. *Nitrosation Reactions and the Chemistry of Nitric Oxide*; Elsevier B.V.: Amsterdam, 2004.
(17) Markovits, G. Y.; Schwartz, S. E.; Newman, L. *Inorg. Chem.* **1981**, *20*, 445.
(18) Nakabayashi, T.; Kosugi, K.; Nishi, N. *J. Phys. Chem. A* **1999**, *103*, 8595.
(19) Collings, P.; Al-Mallah, K.; Stedman, G. *J. Chem. Soc., Perkin Trans. 2* **1975**, 1734.
(20) da Silva, G.; Dlugogorski, B. Z.; Kennedy, E. M. *Int. J. Chem. Kinetics* **2007**, *39*, 645.
(21) Grossi, L.; Montevecchi, P. C. *J. Org. Chem.* **2002**, *67*, 8625.
(22) Al-Mallah, K.; Collings, P.; Stedman, G. *J. Chem. Soc., Dalton Trans.* **1974**, 2469.
(23) Schiessl, W. C.; Summa, N. K.; Weber, C. F.; Gubo, S.; Dücker-Benfer, C.; Puchta, R.; van Eikema Hommes, N. J. R.; van Eldik, R. *Z. Anorg. Allg. Chem.* **2005**, *631*, 2812.
(24) *ChemAxon*, 5.3.8 ed.; ChemAxon: Cambridge, 2010; Marvin Sketch was used for drawing.
(25) Sandström, J. *Acta Chem. Scand.* **1963**, *17*, 678.
(26) Edward, J. T.; Derdall, G. D.; Wong, S. C. *Can. J. Chem.* **1976**, *55*, 2331.
(27) Collings, P.; Garley, M.; Stedman, G. *J. Chem. Soc., Dalton Trans.* **1981**, 331.
(28) Garley, M. S.; Stedman, G.; Miller, H. *J. Chem. Soc., Dalton Trans.* **1984**, 1959.
(29) *Lange's Handbook of Chemistry*, 13th ed.; Dean, J. A., Ed.; McGraw Hill Book Co.: New York, 1984.
(30) Alberty, R. A. *Thermodynamics of Biochemical Reactions*; John Wiley & Sons, Inc.: New York, 2005.
(31) Stedman, G.; Whincup, P. A. E. *J. Chem. Soc.* **1963**, 5796.
(32) Matsumura, K.; Enoki, Y.; Kohzuki, H.; Sakata, S. *Jpn. J. Physiol.* **1990**, *40*, 567.
(33) Ridd, J. H. *Advances in Physical Organic Chemistry*; Gold, V., Bethell, D., Eds.; Academic Press: New York, 1978; Vol. *16*, pp 1−49.
(34) Becker, K. H.; Kleffmann, J.; Kurtenbach, R.; Wiesen, P. *J. Phys. Chem.* **1996**, *100*, 14984.
(35) Seel, F.; Winkler, R. *Z. Phys. Chem.* **1960**, *25*, 217.
(36) Timerghazin, Q. K.; Peslherbe, G. H.; English, A. M. *Phys. Chem. Chem. Phys.* **2008**, *10*, 1532.
(37) Ruano, C.; Otero, J. C.; Arenas, J. F.; Soto, J. *Chem. Phys. Lett.* **2012**, *553*, 17.
(38) Fukui, K.; Yonezawa, T.; Shingu, H. *J. Chem. Phys.* **1952**, *20*, 722.
(39) Parr, R. G.; Yang, W. *J. Am. Chem. Soc.* **1984**, *106*, 4049.
(40) Hirshfeld, F. L. *Theor. Chim. Acta* **1977**, *44*, 129.
(41) Werner, E. A. *J. Chem. Soc., Chem. Commun.* **1912**, 2180.
(42) Nakatani, H.; Hiromi, K. *J. Biochem.* **1980**, *87*, 1805.
(43) Rosenthal, D.; Taylor, T. I. *J. Am. Chem. Soc.* **1960**, *82*, 4169.
(44) Kuzmič, P. *Anal. Biochem.* **1996**, *237*, 260.
(45) Rayson, M. S.; Mackie, J. C.; Kennedy, E. M.; Dlugogorski, B. Z. *Inorg. Chem.* **2011**, *50*, 7440.
(46) Toth, A. M.; Liptak, M. D.; Phillips, D. L.; Shields, G. C. *J. Chem. Phys.* **2001**, *114*, 4595.
(47) Tissandier, M. D.; Cowen, K. A.; Feng, W. Y.; Gundlach, E.; Cohen, M. H.; Earhart, A. D.; Coe, J. V.; Tuttle, T. R. *J. Phys. Chem. A* **1998**, *102*, 7787.
(48) Rayson, M. S.; Mackie, J. C.; Kennedy, E. M.; Dlugogorski, B. Z. *Inorg. Chem.* **2012**, *51*, 2178.
(49) Lewars, E. G. *Computational Chemistry: Introduction to the Theory and Applications of Molecular and Quantum Mechanics*; Kluwer Academic Publishers: Dordrecht, The Netherlands, 2004.
(50) Marenich, A. V.; Olson, R. M.; Kelly, C. P.; Cramer, C. J.; Truhlar, D. G. *J. Chem. Theory Comput.* **2007**, *3*, 2011.
(51) Marenich, A. V.; Cramer, C. J.; Truhlar, D. G. *J. Phys. Chem. B* **2009**, *113*, 4538.
(52) Guthrie, J. P. *J. Phys. Chem. B* **2009**, *113*, 4501.
(53) Frisch, M. J.; Trucks, G. W.; Schlegel, H. B.; Scuseria, G. E.; Robb, M. A.; Cheeseman, J. R.; Scalmani, G.; Barone, V.; Mennucci, B.; Petersson, G. A.; Nakatsuji, H.; Caricato, M.; Li, X.; Hratchian, H. P.; Izmaylov, A. F.; Bloino, J.; Zheng, G.; Sonnenberg, J. L.; Hada, M.; Ehara, M.; Toyota, K.; Fukuda, R.; Hasegawa, J.; Ishida, M.; Nakajima, T.; Honda, Y.; Kitao, O.; Nakai, H.; Vreven, T.; Montgomery, J. A., Jr.; Peralta, J. E.; Ogliaro, F.; Bearpark, M.; Heyd, J. J.; Brothers, E.; Kudin, K. N.; Staroverov, V. N.; Kobayashi, R.; Normand, J.; Raghavachari, K.; Rendell, A.; Burant, J. C.; Iyengar, S. S.; Tomasi, J.; Cossi, M.; Rega, N.; Millam, J. M.; Klene, M.; Knox, J. E.; Cross, J. B.; Bakken, V.; Adamo, C.; Jaramillo, J.; Gomperts, R.; Stratmann, R. E.; Yazyev, O.; Austin, A. J.; Cammi, R.; Pomelli, C.; Ochterski, J. W.; Martin, R. L.; Morokuma, K.; Zakrzewski, V. G.; Voth, G. A.; Salvador, P.; Dannenberg, J. J.; Dapprich, S.; Daniels, A. D.; Farkas; Foresman, J. B.; Ortiz, J. V.; Cioslowski, J.; Fox, D. J. *Gaussian 09*; Gaussian: Wallingford, CT, 2009.
(54) Delley, B. *J. Chem. Phys.* **2000**, *113*, 7756.

DOI: 10.1021/acs.joc.5b00313
J. Org. Chem. 2015, 80, 6951−6958